

## Supporting Information

### **In-situ Vulcanization Synthesis of CuInS<sub>2</sub> Nanosheet Arrays for Memristor with High On-off Ratio and Low Power Consumption**

Zijun Hu<sup>‡a</sup>, Fa Cao<sup>‡a,b</sup>, Tingting Yan<sup>a</sup>, Li Su<sup>a,b</sup> and Xiaosheng Fang<sup>\*a</sup>

<sup>a</sup> Department of Materials Science, State Key Laboratory of Molecular Engineering of Polymers, Fudan University, Shanghai 200433, P. R. China. E-mail: xshfang@fudan.edu.cn

<sup>b</sup> Zhangjiang Fudan International Innovation Center, Shanghai 201210, P. R. China.

<sup>‡</sup> These authors contributed equally to this work.

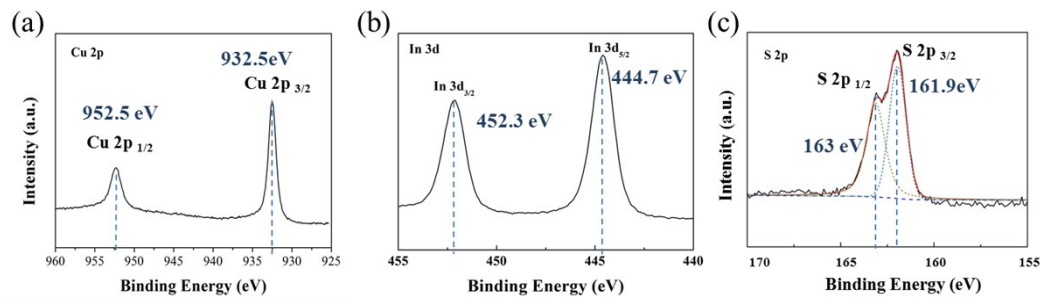


**Figure S1.** XPS spectra of the CuInS<sub>2</sub> nanosheet arrays with elements spectra of a) Cu, b) In and c) S.

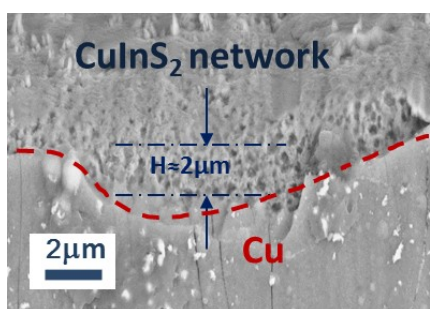


**Figure S2.** Cross-sectional SEM view of the CIS film on Cu copper.

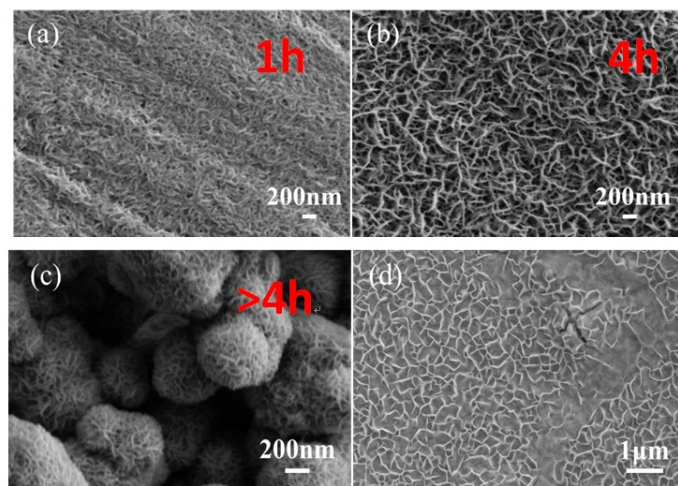


**Figure S3.** Morphologies of two types of copper substrates with different stage of reaction time in solution. a) SEM of purchased 0.5 mm pure copper sheet after vulcanized time of 1 h. b) SEM of vulcanization time of 4 h on copper sheet same as a). c) SEM of vulcanization time of 5 h on copper sheet same as a). d) SEM of vapor deposition of 5  $\mu$ m Copper substrate followed with vulcanized time of 1 h.

By contrast, the growth process could be learned that at the initial stage (1 h), the copper substrate is etched to show the shallow and thick strip patterns (Figure S3a), which cover all over the surface of Cu sheet within the solution to outline the dense nanosheet edges. As the etching time (i.e. vulcanized time) increases, those nanosheets grow larger hence viewed less denser in Figure S3a and with nano-thickness less than 50 nm, and apparent interconnecting structures appeared as Figure S3b exhibits. While with time further increasing to the second stage (time > ~ 4 h), massive flower-sphere structure made of CIS chips formed and spread all over the as-formed bottomed CIS film, distributed randomly with an average diameter of 3  $\mu\text{m}$ . The apparent contrast is illustrated in Figure S6.

Actually, there are two growth mechanisms could be explained corresponding to the two stages. When the reaction time is relatively short, the ions in the solution contact with the substrate and mainly undergo heterogeneous nucleation based on the roughness fluctuates on the copper sheet surface resulting in the formation of uniform CIS nanosheet network layer. As the reaction time increases, the CIS nanosheets nucleation tend to saturated on the surface and are overcrowded aligned. Then, at most local sites, in addition to the heterogeneous nucleation on the substrate surface, the homogeneous nucleation process will also occur in the solution and form the nanoflower ball structure with ions deriving from all the directions, followed by deposition and assembly on the underlying heterogeneous nucleated CIS nanoarrays, the growth kinetics of which is also called the Ostwald Ripening mechanism. In addition, it should be noted that the roughness of copper would have impacts on the synthesized process. The rough surface would offer massive nucleated sites for the CIS growth, resulting in more dense nanoarray of CIS. In this work, as all the copper sheets used are directly purchased as 0.5 mm thickness manufactured by machining processing, which possess evident oriented rolling processing strips in micro scale though after acid cleaning, which could be clearly seen in film forming primary stage as Figure S3a. To prove that the roughness plays an important role in the nucleation process, we evaporated 5  $\mu\text{m}$  thickness copper on glass substrate and dipped into

solution for equal time vulcanization compared with copper sheet, the deposited copper with smoother surface would lead to a much more sparse nanosheet array of the CIS film (Figure S3a vs. Figure S3d) because of fewer nucleation sites. This finding could also in turn prove the growth mechanism of heterogeneous nucleation process happened on the copper.

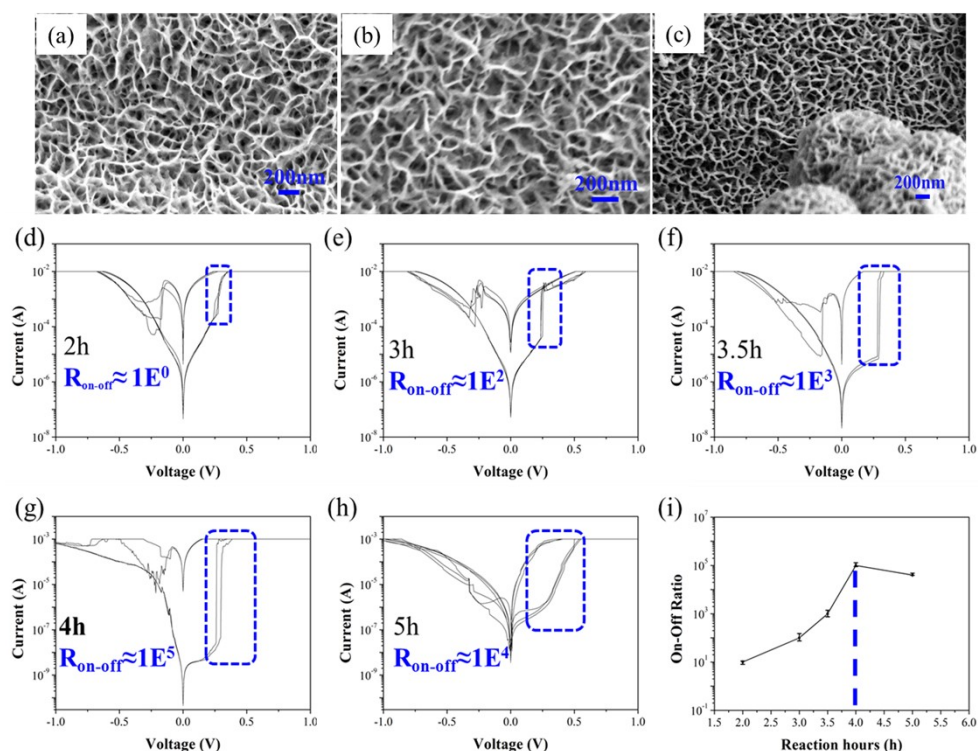


**Figure S4.** The comparison of synthesized time of 2 h, 3 h, 3.5 h, 4 h, 5 h to illustrate the effects on memristor properties. a-c) SEM morphology images of 2 h, 4 h and 5 h with 200 nm scale. d-h) I-V characterization of the series of time of 2 h in d), 3 h in e), 3.5 h in f), 4 h in g) and 5 h in h). i) The  $R_{ON}/R_{OFF}$  ratio statistics of the above time-dependent samples.

In order to further explore the relationship between the synthesis craft and materials properties, we have controlled a patch of samples with a series of gradient reaction time of vulcanization (2 h, 3 h, 3.5 h, 4 h, 5 h) and have tested the corresponding I-V characteristics as contrasted in Figure S4. Form Figure S4a to S4c, it is clearly observed that with the reaction time increasing, the vertical nanosheets become larger and crowded to constitute the uniform CIS film till ~4 h, then lots of superstructure of flower-sphere show up to cover the CIS film as a second layer.

Actually, as the larger scale SEM in Figure S6c indicates, few sphere structures could also be formed at the first stage, which probably is resulted by the solution concentration fluctuations.

In terms of the memristive properties, we have tested 10 devices for each reaction time, and evenly evaluated the values of on-off ratio of these time-dependent CIS films in Figure S4(d-i), it turns out that the memory window displays an expanding trend as CIS grow larger till the 4 h samples, especially the 5 h CIS sample exhibits an apparent slow set operation process with sloping resistive switching comparing with the other group samples. For further explanation, we have characterized the cross section fragments of these samples by half-folding the copper sheets back and forth then cut off as Figure S5 shows, the maximum thickness of these cracks at each group shows an increasing trend as reaction time prolonged as Figure S5 a-d shows, which means that the obtained larger nanosheets would require a longer channel to form conduction fibre leading to bigger on-off ratio. However when quantities of flower-sphere structures formed above the bottom CIS layer, the original threshold voltage would be unable enough to achieve the resistive switching, thus resulting in a slow set operation process, and larger operation power is demanded for memristive behaviors.

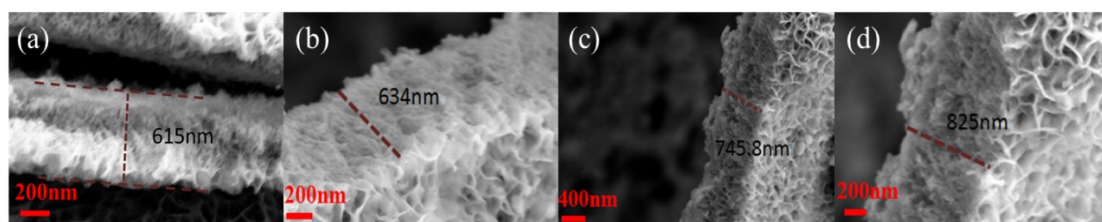


**Figure S5.** The cross section fragments of these samples under reaction time of 2 h in a), 3 h in b), 3.5 h in c) and 4 h in d).

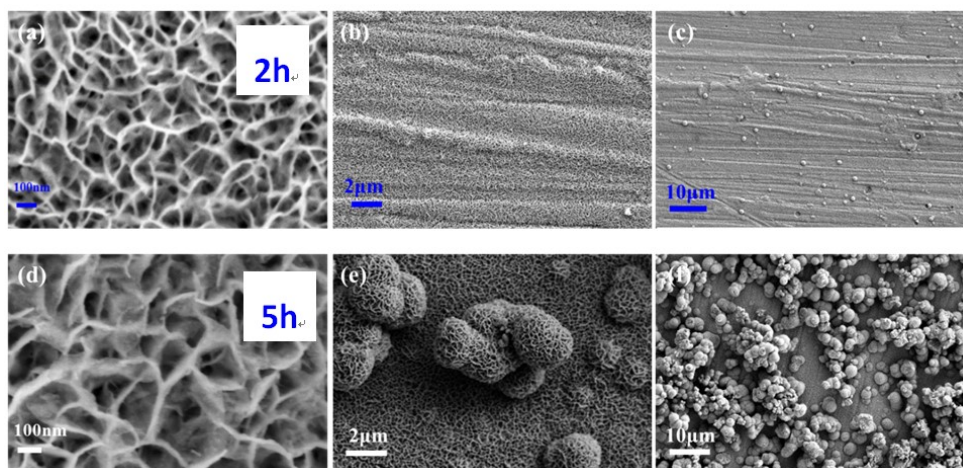


**Figure S6.** The reaction time of 2 h in a), b) and c) with different scale shows hetero-nucleation process. The reaction time of 5 h with main sphere structure in d), e) and f) with varied scale view by Ostwald ripening growth mechanism.

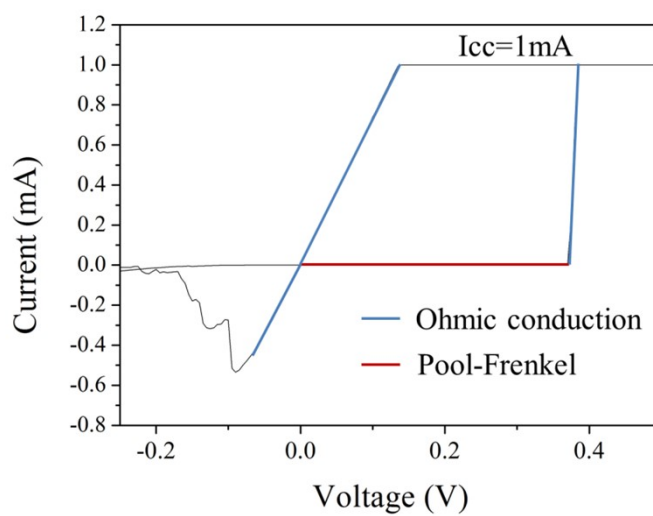


**Figure S7.** The entire process of the bipolar memristive switching mechanism of CIS.

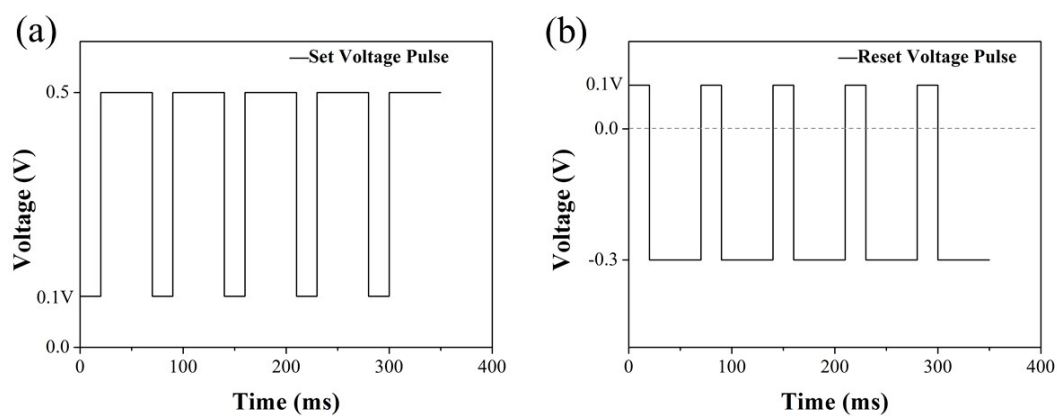


**Figure S8.** The writing pulses and erasing pulses level of a) 0.5 V/0.1 V for Set/Read. b) -0.3 V/0.1 V for Reset/Read.

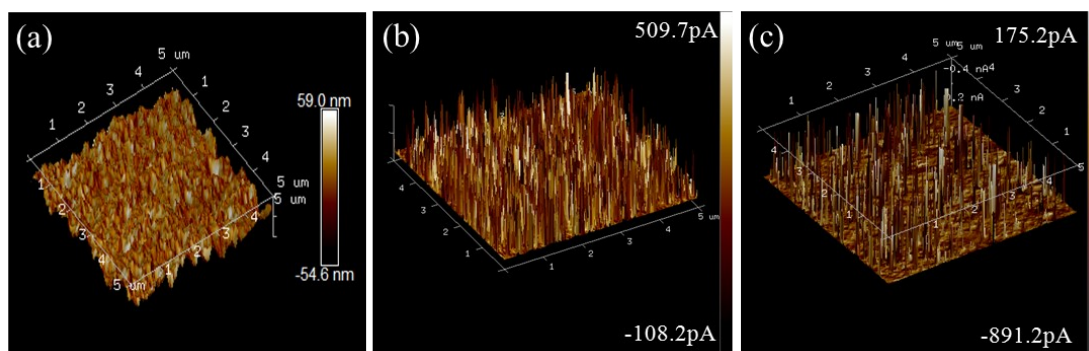


**Figure S9** a) 3D surface morphology AFM image of 5 μm x 5 μm area. b) 3D C-AFM current distributing mapping at voltage of 0.5V. c) 3D C-AFM current distributing mapping at voltage of -0.3V.

**Table S1.** EDX results of CuInS<sub>2</sub> shows that the atomic percent of In:S is around 1:2.

Element	Wt%	Atomic%
S	13.76	26.57
Cu	61.78	60.23
In	24.46	13.20
<b>Total</b>	<b>100</b>	<b>100</b>

**Table S2.** Comparison of the main parameters of the other chalcogenides-based memristor in the literature.

Device	On-Off Ratio	Threshold voltage (V)	Retention time (s)	Endurance (cycle)	Type	Ref
Ag/Ag-Ag <sub>2</sub> S/Pt	10 <sup>4</sup>	0.1-0.2/-0.25	-	-	Bipolar	1
Ta/Sb <sub>2</sub> Te <sub>3</sub> /Ta	2.4	1.3/-1	-	-	Bipolar	2
Au/In <sub>2</sub> S <sub>3</sub> /Au	10 <sup>5</sup>	6/-6	10 <sup>4</sup>	200	Bipolar	3
Cu/Cu <sub>2</sub> S/Pt	11.4	0.7/-2	-	-	Bipolar	4
/TiO <sub>2</sub> /SiO <sub>2</sub> /Si						
Ti/HfSe <sub>x</sub> O <sub>y</sub> /HfSe <sub>2</sub> /Au	10 <sup>3</sup>	2.32/-0.7	>15000	40	Bipolar	5
Ag/Ag-GeTe/TiW	~10 <sup>4</sup>	~0.2/-0.2	-	4	Bipolar	6
Pt/CuInSe <sub>2</sub> /Al <sub>2</sub> O <sub>3</sub> /Si	10 <sup>3</sup>	~2/-2	-	10	Bipolar	7
Ag/AgInSbTe/Ag	~7	0.11-0.4/-0.22	>600	-	Bipolar	8
Mo/GeSbTe/Ag	~2	0.8/-0.75	-	100	Bipolar	9
Pt/GeS/Te	>10 <sup>3</sup>	0.9-2.1/0.29-0.47	-	20	Unipolar	10
Ti/Ge <sub>2</sub> Sb <sub>2</sub> Te <sub>3</sub> /Pt	>10 <sup>2</sup>	0.9-2/-1	>10 <sup>4</sup>	100	Bipolar	11
<b>Cu/CuInS<sub>2</sub>/Au</b>	<b>10<sup>6</sup></b>	<b>~0.3/-0.3</b>	<b>&gt;10<sup>4</sup></b>	<b>&gt;600</b>	<b>Bipolar</b>	<b>This Work</b>

### Reference

- 1 N. V Khan, M. M. Burkitbayev, F. Kh, A. Saengsonachai, Y. Seekaew, P. Traiwatcharanon, C. Liang, K. Terabe, T. Hasegawa and M. Aono, *Nanotechnology*, 2007, **18**, 5.
- 2 J. J. Zhang, N. Liu, H. J. Sun, P. Yan, Y. Li, S. J. Zhong, S. Xie, R. J. Li and X. S. Miao, *J. Electron. Mater.*, 2016, **45**, 1154–1159.

- 3 Y. Zhao, D. Yu, Z. Liu, S. Li and Z. He, *IEEE Access*, 2020, **8**, 106726–106734.
- 4 B. Yang, H. X. Guo, K. B. Yin, Y. D. Xia, L. Chen, J. Yin and Z. G. Liu, *J. Electroceramics*, 2009, **22**, 87–90.
- 5 L. Liu, Y. Li, X. Huang, J. Chen, Z. Yang, K. H. Xue, M. Xu, H. Chen, P. Zhou and X. Miao, *Adv. Sci.*, 2021, **8**, 2005038.
- 6 C.-J. Kim, S.-G. Yoon, K.-J. Choi, S.-O. Ryu, S.-M. Yoon, N.-Y. Lee and B.-G. Yu, *J. Vac. Sci. Technol. B Microelectron. Nanom. Struct.*, 2006, **24**, 721.
- 7 T. Ahmad, W. Devulder, K. Opsomer, M. Minjauw, U. Celano, T. Hantschel, W. Vandervorst, L. Goux, G. S. Kar and C. Detavernier, *ACS Appl. Mater. Interfaces*, 2018, **10**, 14835–14842.
- 8 J. J. Zhang, H. J. Sun, Y. Li, Q. Wang, X. H. Xu and X. S. Miao, *Appl. Phys. Lett.*, 2013, **102**, 183513.
- 9 R. Pandian, B. J. Kooi, J. L. M. Oosthoek, P. Van Den Dool, G. Palasantzas and A. Pauza, *Appl. Phys. Lett.*, 2009, **95**, 252109.
- 10 Z. Zhang, Y. Wang, Y. Luo, Y. He, M. Ma, R. Yang and H. Li, *Sci. Rep.*, 2018, **8**, 1–9.
- 11 S. Yoo, T. Eom, T. Gwon and C. S. Hwang, *Nanoscale*, 2015, **7**, 6340–6347.